LIFETIME EVALUATION OF A THREE-PHASE PHOTOVOLTAIC INVERTER DURING HARMONIC CURRENT COMPENSATION

Rodrigo Cassio de Barros[1], Wallace do Couto Boaventura[1] Heverton Augusto Pereira[2], Allan Fagner Cupertino[3]

[1]Graduate Program in Electrical Engineering, Federal University of Minas Gerais, Belo Horizonte, MG, Brazil

[2]Department of Electrical Engineering, Federal University of Viçosa, Viçosa, MG, Brazil

[3]Department of Materials Engineering, Federal Center for Technological Education of Minas Gerais, Belo Horizonte, MG, Brazil

***Abstract* – The Photovoltaic (PV) inverters operating with ancillary service capability have been discussed as a solution to improve the power quality of the electrical grid. In this context, the PV inverters can be used to provide services such as Harmonic Current Compensation (HCC). However, the analysis of how much this extra functionality can affect the reliability of the PV inverter is necessary. Thus, this work analyzes the lifetime of a three-phase PV inverter taking into account the degradation of the semiconductor devices (IGBTs and diodes) and the dc-link capacitors. The compensation of the 5^{th} and 7^{th} harmonic current components (and their combination) are considered. The lifetime evaluation is performed based on an mission profiles of solar irradiance, ambient temperature, harmonic current amplitude and phase-angle. Based on the results of the adopted case study, the HCC operation increases the lifetime consumption of the IGBTs, diodes and dc-link capacitors. Compared to traditional PV inverter operation, The results reveals a reduction in the predicted B_{10} lifetime of 3.4 and 4.1 years, when the PV inverter compensates 5th and 7th harmonic, respectively. The reduction is even more significant (5.6 years) when the 5^{th} and 7^{th} harmonic component are simultaneously compensated.**

***Keywords* – PV inverter, Ancillary services, Harmonic current compensation, Lifetime evaluation.**

I. INTRODUCTION

The Renewable Energy (RE) power capacity was greater than 256 Gigawatts (GW) in 2020, achieving another record-breaking year [1]. In this context, Photovoltaic (PV) and wind power systems have installed a record amount of new capacity and they are leading this growth. According to [1], auctions and tenders for renewable power have become one of the most common market support mechanisms for new projects in 2020 and 13 countries awarded nearly 50 GW of RE in new capacity.

The PV systems can be used to inject active power to the grid (traditional operation) or they can be used to perform ancillary services (multifunctional operation). In this scenario, multifunctional PV inverters have been strongly discussed in the literature as an alternative to improve the grid power quality [2], [3], [4], [5]. In this operation mode, the PV inverter provides ancillary services when it is operating below its nominal active power specification. Some examples of the ancillary services are the Harmonic Current Compensation (HCC), reactive power injection and grid frequency regulation [6], [7].

Manuscript received 12/08/2021; first revision 01/17/2021; accepted for publication 05/05/2022, by recommendation of Editor Marcelo Lobo Heldwein.

Some references in the literature have stated the lifetime evaluation of the multifunctional inverter operating with reactive power compensation [6], [8], [9]. In addition, the lifetime evaluation for a single-phase PV inverter operating with HCC was proposed by [10]. However, only the long cycle lifetime analysis was performed in this work. In reference [11], the lifetime evaluation for a single-phase PV inverter with HCC including the long and short cycles analysis were presented. However, reference [10] and [11] do not analyze the effect of the HCC operation for a three-phase PV inverter and do not consider the lifetime evaluation of the diodes and dc-link capacitors. Therefore, a study to analyze the diodes and dc-link capacitor lifetime during the HCC operation is necessary, since these components are considered one of the most prone to failure components in PV inverters [12].

This work is outlined as follows: section II describes the three-phase PV system with HCC operation, focusing on the control strategy and section III presents the lifetime evaluation methodology for the semiconductor devices. Section IV describes the effect of HCC operation mode on the dc-link capacitors. In section V, a case study to perform the lifetime evaluation of a three-phase PV inverter is presented. Section VI presents the results of PV inverter lifetime consumption during the HCC operation mode and the conclusions are stated in section VII.

II. THREE-PHASE PV INVERTER WITH HCC OPERATION

A typical three-phase PV inverter is presented in the Figure 1. As observed, the PV modules are connected to the inverter dc-link. In addition, an LCL filter is used to attenuate the high harmonic frequencies due to the switching process of the semiconductor devices in the PV inverter. Also, an non-linear load is connected to the Point of Common Coupling (PCC). In the evaluated scenario, the PV inverter compensates the harmonics generated by the non-linear load.

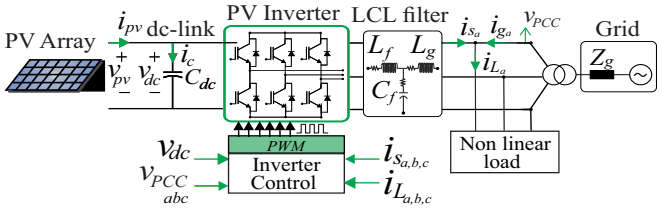

Fig. 1. Typical three-phase PV inverter connected into the electrical grid.

The control strategy used in this work is presented in Figure 2. Since the HCC operation mode is implemented, the control strategy is based on the stationary coordinates ($\alpha\ \beta 0$). As observed, there are the inner and outer loops. The inner loop controls the output current of the PV inverter. The outer loop controls the dc-link voltage. The dc-link voltage reference (v_{dc}^*) is provided by the Maximum Power Point Tracking (MPPT) algorithm. Thus, the active power reference (P^*) is calculated based on the energy stored in the dc-link capacitor and the reactive power reference (Q^*) is considered equal to zero. The fundamental current references ($i_{s'\alpha}$, $i_{s'\beta}$) are provided based on the Instantaneous Power Theory (IPT) [13]. Thus, the load current components ($i_{L\alpha}$, $i_{L\beta}$) are added to the inverter current and the reference currents of the inverter ($i_{s\alpha}^*$, $i_{s\beta}^*$) are generated. A Proportional Multi-resonant Controller (PMR) is used to control the inverter current. The tunning procedure is discussed in details by reference [14]. Thus, Clarke transformation is used and the SVPWM is adopted as the modulation strategy of the system.

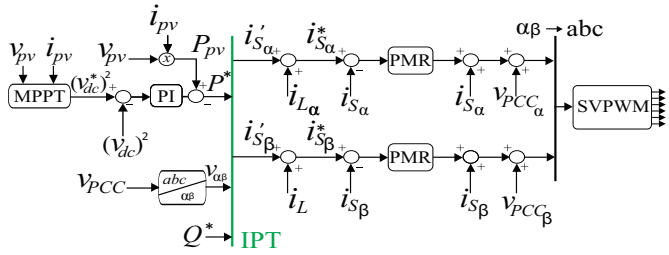

Fig. 2. Block diagram of the PV inverter control strategy.

The control strategy was implemented in an experimental bench. Thus, a power module of 10 kW, manufactured by Semikron, was used in this work. The dc-link voltage equal to 450 V was taken as reference and the inverter was connected to electrical grid of 220 V RMS (line to line). In addition, an L filter (1.8 mH) was used in the experimental bench instead of an LCL filter. , due to the resources availability when the experiments were conducted. The output current of the inverter is presented in Figure 3. In this case, the reference of the inverter current was performed to obtain an injection of 6 A of fundamental current and: 2 A of 5^{th} harmonic component with phase-angle 180^o in Figure 3(b), 2 A of 7^{th} harmonic component with phase-angle 180^o in Figure 3(c) and 2 A of 5^{th} and 7^{th} harmonic components with phase-angle 180^o in Figure 3(d). In addition, in Figure 3(a) only the injection of the 6 A of fundamental current is performed. The harmonic spectrum of the inverter current output is presented in Figure 4.

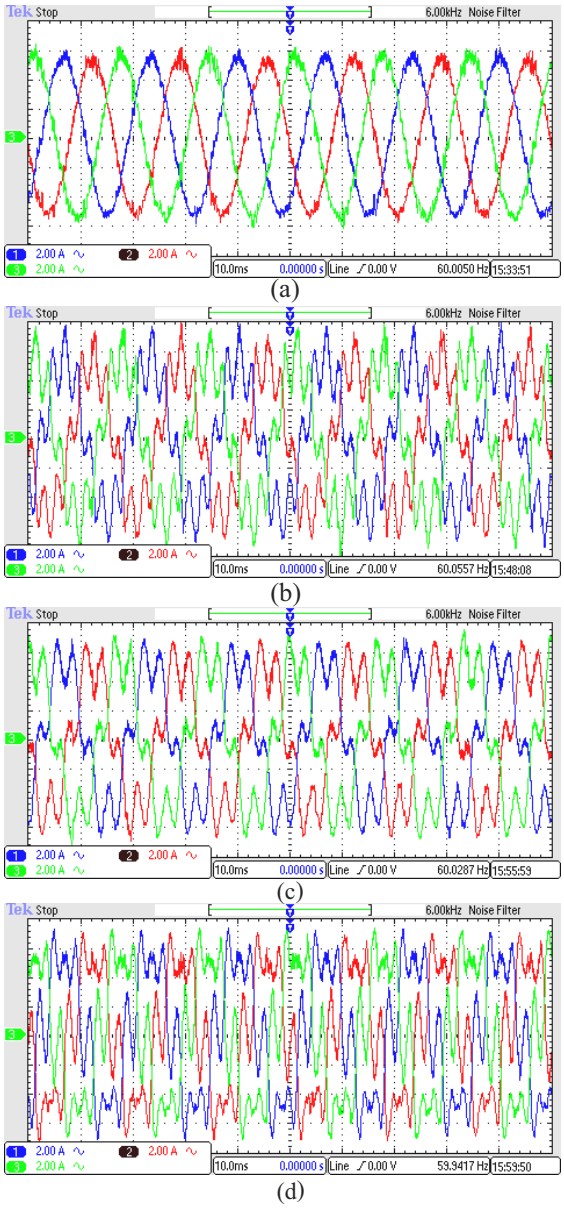

Fig. 3. Output current of a three-phase PV inverter injecting: (a) 6 A of I_f and: (b) 2 A of I_5 with $\theta_h = 180°$, (c) 2 A of I_7 with $\theta_h = 180°$ and (d) 2 A of I_5 and I_7 with $\theta_h = 180°$.

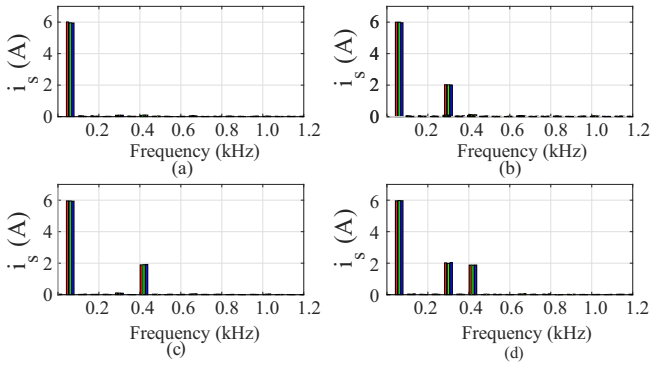

Fig. 4. Spectrum current of a three-phase PV inverter injecting: (a) 6 A of I_f and: (b) 2 A of I_5 with $\theta_h = 180°$, (c) 2 A of I_7 with $\theta_h = 180°$ and (d) 2 A of I_5 and I_7 with $\theta_h = 180°$.

III. THE EFFECT OF THE HCC OPERATION ON THE SEMICONDUCTORS DEVICES

Before understand the effect of the HCC process in the inverter lifetime, it is important to understand how the inverter output current is synthesized. Considering the compensation of the harmonic component (h) with the highest amplitude (I_h), the output current for phase a ($i_{sa}(t)$) can be presented as:

$$i_{sa}(t) = I_f \cos(\omega_f t) + I_h \cos(h\omega_f t + \theta_h), \quad (1)$$

where I_f is the amplitude of the fundamental component, ω_f is the angular grid frequency and θ_h is the harmonic current phase-angle. As observed, the PV inverter output current of the dc/ac stage depends on the harmonic current parameters (h, I_h, and θ_h). As an example, the current signals of dc/ac stage compensating 5^{th} harmonic component with phase-angles 0° and 180° are shown in Figure 5(a).

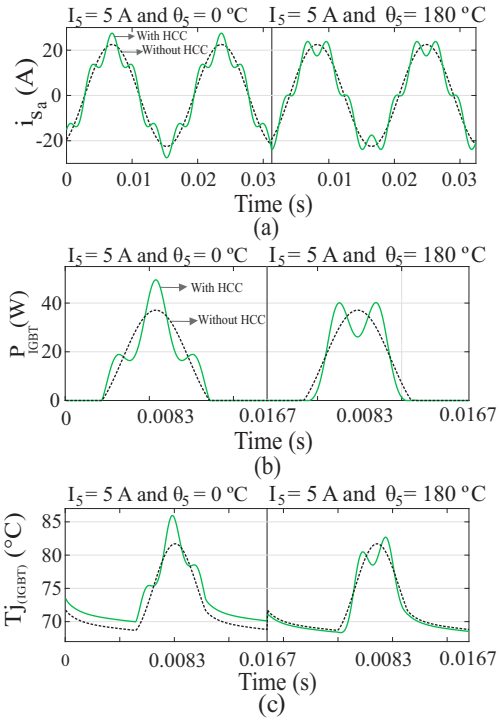

Fig. 5. PV inverter injecting 21.5 A of fundamental current and 5 A of 5^{th} harmonic component: (a) Inverter current output (phase a); (b) Power losses of the IGBT and (c) Junction temperature of the IGBT.

The lifetime evaluation of the semiconductor devices has been discussed in recent works [15], [16], [17]. In this context, the Physics-of-Failure (PoF) methodology has been constantly used in the lifetime evaluation of power electronics. The PoF can provide different reliability models based on the strength and stress in which the component is submitted. With regarding to the semiconductor devices, the meam junction temperature (T_{jm}), the fluctuation junction temperature (ΔT_j) and the heating time (t_{on}) are dressed as the most stress factors in the semiconductor devices.

Since the shape of the output current is affected by the HCC operation, the power losses and consequently the junction temperature of the semiconductor devices are also affected. In Figure 5(b) and (c), the power losses of an IGBT (P_{IGBT}), and the junction temperature of this component ($T_{j\,IGBT}$) are presented. For this specific case, the 5^{th} harmonic component, with phases angle 0° and 180°, are compensated by the PV inverter. As observed, with the HCC operation mode, the junction temperature of the semiconductor devices presents additional power cycling when compared to the traditional PV inverter operation.

The lifetime evaluation of semiconductor devices can be divided as long and short cycle analysis [18]. The long cycle is the lifetime consumption in the component due to the variation of the environment conditions, such as solar irradiance and ambient temperature. The short cycle analysis is the lifetime consumption in the component due to the grid frequency. Therefore, the short cycle lifetime evaluation of the semiconductor devices when the inverter works with HCC operation is not a straightforward task, since there is additional power cycling due to the harmonic frequencies. Thus, it is necessary a methodology to take into account all the additional power cycling in the junction temperature due the fundamental and harmonics frequencies.

The methodology proposed by [11] was considered in this work. In this reference, the methodology for short and long cycles were proposed and applied to IGBTs of single-phase PV inverter. The flowchart for the long and short cycle analysis are presented in Figure 6(a) and (b), respectively.

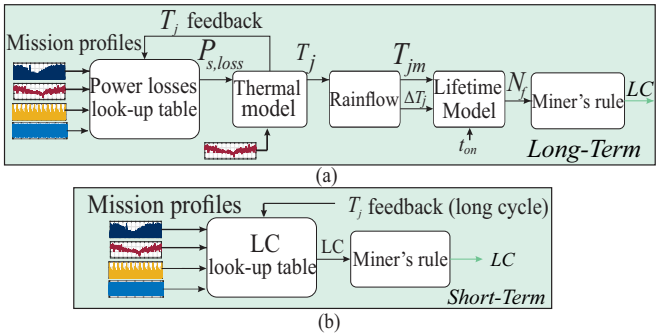

Fig. 6. Flowchart for the lifetime evaluation of the semiconductor devices: (a) long cycle and (b) short cycle.

For the long cycle analysis, the mission profiles of the PV inverter operation are used as the input to estimate the annual power losses of the semiconductor devices. Thus, the mission profile of solar irradiance, ambient temperature, harmonic amplitude and phase-angle are used. The mission profiles are applied to the power losses look-up table and the annual power losses are estimated. The power losses look-up table was previously created in a simulation environment varying the input parameters, which are the same parameters of the mission profile. In addition, the manufacturer information provided on the datasheet are used and the conduction and switching power losses are calculated.

The power losses are translated to the semiconductor devices junction temperature by a electrical thermal model. Thus, a thermal model based on Cauer and Foster models are used in this work [19]. Therefore, the annual junction temperature for the semiconductor devices are obtained. The junction temperature are then applied to the rainflow counting algorithm to estimate the regular parameters of T_{jm}, ΔT_j and t_{on} [20].Therefore, these parameters are applied to the lifetime model, proposed by [21]:

$$N_f = A(\Delta T_j)^{\alpha}(ar)^{\beta_1 \Delta T_j + \beta_0}\left[\frac{C+(t_{on})^{\gamma}}{C+1}\right]\exp\left(\frac{E_a}{k_b T_{jm}}\right) f_d, \quad (2)$$

where the meaning and values of the parameters A, α, β_1, β_0, C, γ, E_a and f_d are defined in [21]. k_b is the Boltzmann constant and ar equal to 0.35 is used in this work. Besides, the parameter f_d is equal to to calculate the N_f of IGBTs, as proposed by [21].

The lifetime evaluation for the short cycle analysis is presented in Figure 6(b). As observed, the same mission profiles used in the long cycles analysis are used. However, for the short cycle analysis, there is a *LC* look-table instead of a power losses look-up table. Basically, the idea is to obtain the main input parameters of the lifetime models (T_{jm}, ΔT_j and t_{on}) directly from the junction temperature waveform of the semiconductor devices (in a simulation environment). More information about the process can be found on reference [11]. Thus, the same lifetime model of Eq. 2 is used to estimate the number of cycle until failure for the short cycle analysis.

Since the lifetime consumption for the long and short cycle are calculated, the damage accumulation is performed. The Miner's rule is used in this work, represented as follows [22]:

$$LC = \sum_k \left(\frac{1}{N_{f,l(k)}} + \frac{T_s \times f_n}{N_{f,s(k)}}\right), \quad (3)$$

where indexes l and s correspond to the long and short thermal cycling, respectively. T_s is the sample time of the mission profile. As observed, the power devices *LC* is given by a cumulative sum of the damages caused by the long and short cycles.

IV. THE EFFECT OF THE HCC OPERATION ON THE DC-LINK CAPACITOR

The HCC operation also affects the current waveform of the dc-link capacitor. Figure 7 presents the capacitor current and its spectrum for the PV inverter working as traditional operation and when the 5^{th} and 7^{th} harmonic components (with phase-angle 0°) are compensated. As observed, low harmonic components are presented in the dc-link current when the HCC operation is performed. This fact increases the capacitor power losses, which are directly related to the capacitor current. In addition, the magnitudes of the harmonic components in the capacitor current vary depending of the harmonic order which is compensated by the PV inverter. Additional tests were performed and it was observed that the magnitudes of the harmonic components in the capacitor current also vary with the variation of the harmonic phase-angle which is compensated by the PV inverter.

The lifetime evaluation of the dc-link capacitor is also similar to the one used in the semiconductor devices, since the mission profiles are taking into account. Furthermore, the power losses of the component are also translated to temperature profiles, which are used in the lifetime evaluation process. The capacitor power losses estimation based on the electrical thermal model is presented in Figure 8.

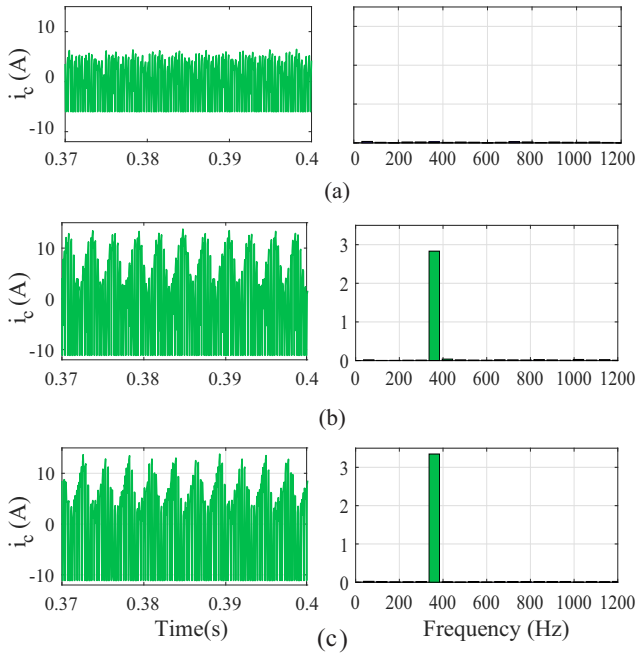

Fig. 7. Dc-link capacitor current waveform and current spectrum when the PV inverter injects 10 A of fundamental current with: no harmonic content injection (a), 2 A of 5^{th} harmonic (b) and 2 A of 7^{th} harmonic (c).

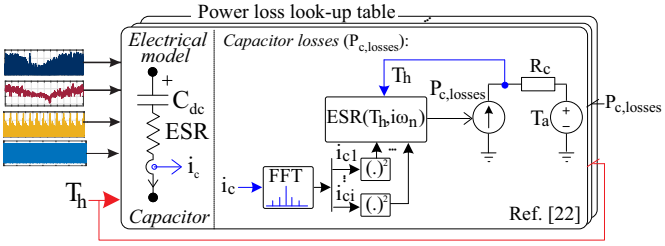

Fig. 8. Flowchart for the capacitor power losses estimation.

Figure 9 summarizes the steps for the lifetime evaluation of dc-link capacitors. The main stress factors are the hot-spot temperature (T_h) and operating voltage (V_c) [12], [23]. The T_h is estimated based on the capacitor power losses, which are calculated as:

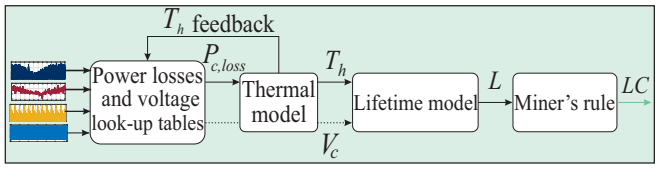

Fig. 9. Flowchart for the lifetime evaluation of dc-link capacitor.

$$P_{c,losses} = \sum_i ESR(T_h, i\omega_n) I^2_{i(RMS)}, \quad (4)$$

where $I_{i(RMS)}$ is the RMS value of each i-th harmonic component of the capacitor current and *ESR* is the capacitor equivalent series resistance. The *ESR* is a function of the capacitor current frequency and the hot-spot temperature, parameters usually provided by the capacitor manufactures [24]. Thus, for the capacitor *ESR* estimation, a look-up table based on the capacitors datasheet information is used. Other approaches to extracting the *ESR* can be found in [25]. Since

TABLE I
Main parameter of the PV system

Parameter	Value
Nominal power	10 kW
Grid voltage (line to line)	220 V
Dc link voltage	450 V
Full-bridge switching frequency	12 kHz
Sampling frequency	12 kHz
Filter inductor - L_f	1.8 mH
Filter inductor - L_g	1.8 mH
Filter capacitor - C_f	3.8 μF
Grid nominal frequency - f_n	60 Hz
Dc-link capacitance - C_{dc}	2040 μ F

the capacitor power losses are computed, T_h can be estimated by [24]:

$$T_h = T_{amb} + R_c P_{c,losses}, \tag{5}$$

where R_c correspond to capacitor equivalent thermal resistance. Then, the time to failure (L) of the capacitor is obtained by [23]:

$$L = L_0 \left(\frac{v_{dc}}{v_0} \right)^{-n} \times 2^{\frac{T_0 - T_h}{10}}, \tag{6}$$

where L_0 is the lifetime under testing conditions. In addition, v_{dc} is the capacitor voltage, v_0 is the rated voltage at test condition and T_0 is the temperature under test condition. As the lifetime of aluminum electrolytic capacitors quite depends on the voltage stress level, the value of the voltage stress exponent n equal to 3 is used in this work, as suggested in [23]. Finally, the capacitor lifetime consumption can be determined by the Miner's rule:

$$LC = \sum_k \left(\frac{T_s}{L_k} \right), \tag{7}$$

where k is the number of samples of the mission profile.

The previous lifetime evaluation methodologies (for the semiconductor devices and capacitor) return a fixed accumulated damage. However, this approach is far from reality, since deviations from model parameters are not considered. Thus, a statistical approach based on Monte Carlo simulation is conducted, according to [18]. The Monte Carlo analysis is simulated for n = 10,000 samples with 5 % of variation over the static values, and the result is fitted using the Probability Density Function (PDF) $f(x)$. The component unreliability is evaluated by the Cumulative Density Function (CDF) $F(x)$, calculated from $f(x)$. The parameters used in the Monte Carlo simulation method are based on the reference [18]. The system wear-out failure probability F_s is obtained with the series-connected reliability model, given by:

$$F_s = 1 - \prod_{j=1}^{n_I} (1 - F_I(x)) \prod_{j=1}^{n_D} (1 - F_D(x)) \prod_{j=1}^{n_C} (1 - F_C(x)), \tag{8}$$

where $F_I(x)$, $F_D(x)$ and $F_C(x)$ are the unreliability functions of the IGBTs, diodes and dc-link capacitor, respectively. n_I, n_D and n_C are the number of IGBTs, diodes and dc-link capacitor in the analyzed system.

V. CASE STUDY

The PV system used in this work is a 10 kW three-phase PV inverter. The main electrical parameters of the system are described in Table I. The used power semiconductor devices are discrete IGBTs 600V/40A (with antiparallel diode) manufactured by Infineon, with part number IKW40N60H3. The dc-link capacitor used is the 680μF/400V, part number B43303 A0687 - M90, manufactured by TDK. The capacitor bank is composed of six dc-link capacitors. They are designed as three strings connected in parallel and each string is composed of two capacitors in series.

The lifetime evaluation of the semiconductor devices and the dc-link capacitor are obtained based on a mission profiles operation of the PV system during one year of operation. The mission profile of solar irradiance (G) and ambient temperature (T_a) were sampled with 1 minute per data in the city of Goiânia, Goiás. These mission profiles are presented in Figure 10(a) - (b).

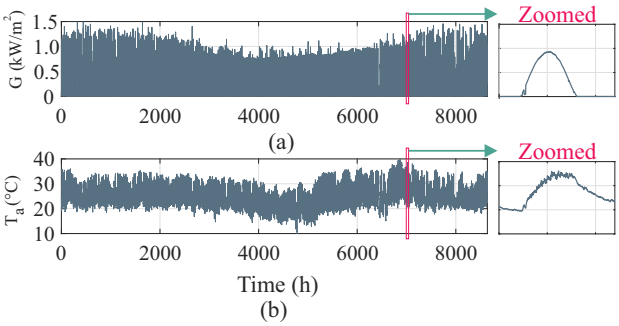

Fig. 10. Mission profile of: (a) Solar irradiance and (b) Ambient temperature.

In addition, mission profiles of the harmonic current amplitude and phase-angle are considered in this work, as presented in Figure 11. The harmonic profiles were measured from a three-phase industry park and also sampled at 1 minute per data. The measurements were performed over one year. The histograms of the mission profiles are also presented in Figure 12.

The 5^{th} and 7^{th} harmonic current components are considered the current distortion in the nonlinear load. These harmonic orders are selected for being very common in three-phase systems, based on studies on electrical systems in different types of commercial facilities [26]. Therefore, four cases are analyzed:

- Case 1: lifetime evaluation of the PV inverter without HCC operation (base case);
- Case 2: lifetime evaluation of the PV inverter injecting only 5^{th} harmonic current component;
- Case 3: lifetime evaluation of the PV inverter injecting only 7^{th} harmonic current component;
- Case 4: lifetime evaluation of the PV inverter when 5^{th} and 7^{th} harmonic current components are injected.

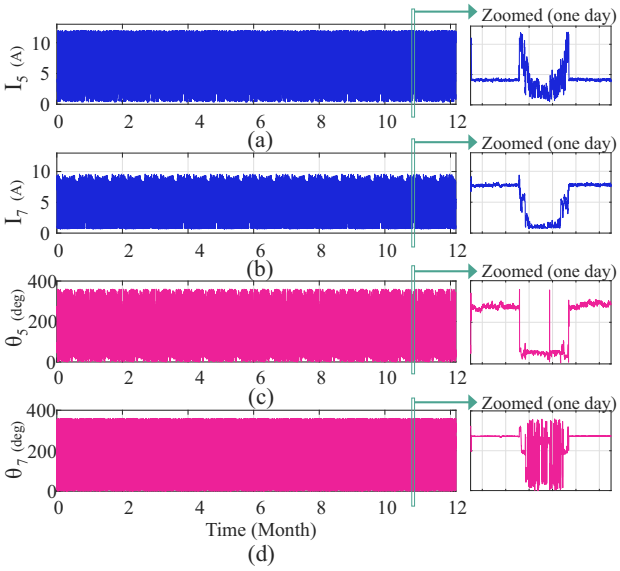

Fig. 11. Mission profile of: (a) 5^{th} harmonic amplitude, (b) 7^{th} harmonic amplitude, (c) 5^{th} harmonic phase-angle and (d) 7^{th} harmonic phase-angle.

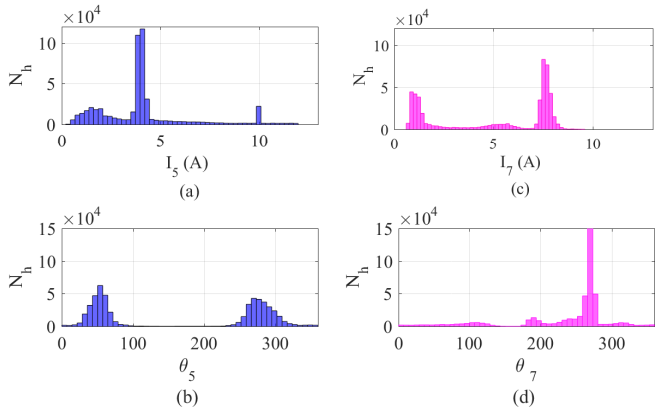

Fig. 12. Mission profile histogram of: (a) 5^{th} harmonic amplitude, (b) 7^{th} harmonic amplitude, (c) 5^{th} harmonic phase-angle and (d) 7^{th} harmonic phase-angle.

The lifetime evaluation for the semiconductors devices and the dc-link capacitor are performed. For the semiconductors devices, the short and long cycles analysis are carried out. Since the lifetime evaluation for the components were estimated, the Monte Carlo simulation considering 10,000 samples was applied to obtain the B_{10} of the system and component levels. The B_{10} is the percentage that 10 % of the samples will probably failure.

VI. RESULTS

The lifetime evaluation for the semiconductor devices and dc-link capacitors are stated in this section. With regarding to the long cycle analysis for the semiconductor devices, part of the power losses look-up table for the IGBTs and diodes are presented in Figure 13. The idea is to observe the effect of the HCC operation on the power losses of the semiconductor devices . Thus, the compensation of the 5^{th} and 7^{th} harmonic current components with different phase-angles and amplitudes combinations are performed. For this specific case, the active power injected by the PV inverter is set at 7 kW and the ambient temperature was set at 25 °C.

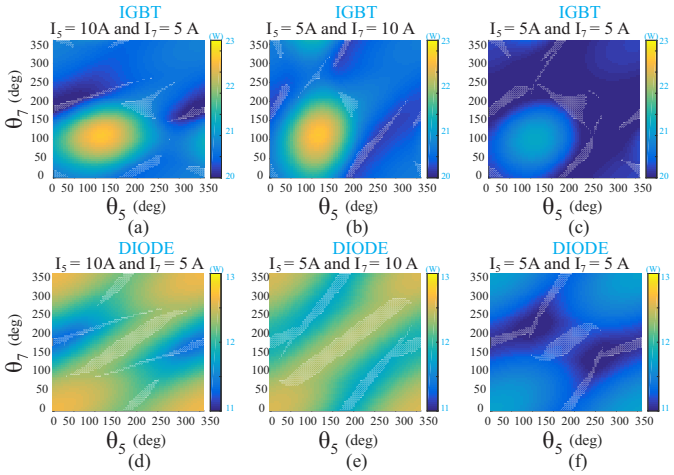

Fig. 13. Power losses for the IGBT when the 5^{th} and 7^{th} harmonic components were compensated considering: (a) I_5 = 10 A and I_7 = 5 A, (b) I_5 = 5 A and I_7 = 10 A and (c) I_5 = 5 A and I_7 = 5 A. For the diodes, the same study were provided: (d) I_5 = 10 A and I_7 = 5 A, (e) I_5 = 5 A and I_7 = 10 A and (f) I_5 = 5 A and I_7 = 5 A.

In Figure 13(a), the PV inverter injects 10 A of 5^{th} harmonic and 5 A of 7^{th} harmonic. As observed, the IGBT power losses present critical values when the phase-angle of the 5^{th} and 7^{th} harmonic components are near to 110°. Similar behavior is observed in Figure 13(b), where the amplitude of the 5^{th} and 7^{th} harmonic components were considered 5 A and 10 A, respectively. In Figure 13(c), the harmonic amplitude for the 5^{th} and 7^{th} harmonic components were both equal to 5 A. In this case, the power losses in the critical area for the IGBT were reduced compared to the previous cases. Thus, it is observed an increasing in the IGBT power losses with the increasing of the harmonic current amplitude. In addition, power losses present critical values for harmonic phase-angles near to 110° (combination of the 5^{th} and 7^{th} harmonic components) .

The same study was performed to the diodes and it is presented in Figure 13(d)-(f). As observed, the power losses also increase with the increasing of the harmonic amplitude. However, critical values of power losses are presented when the 5^{th} and 7^{th} harmonic phase-angles are near to 0° or 360°. This behavior can be explained based on the thermal impedance of the diodes and the thermal cycles presented in the junction temperature of this component.

With regarding to the junction temperature of the semiconductor devices for long cycles analyzes, the mean junction temperature over one year operation is presented in Figure 14. As observed in Case 1, which is the base case, it presents the lowest junction temperature between all the cases. Thus, the HCC operation increases the mean junction temperature for the IGBTs and diodes. In addition, the junction temperature for Case 3 is higher than that for Case 2, which means higher junction temperature when the 7^{th} harmonic component is compensated, compared to the 5^{th} harmonic component. In addition, Case 4, which is the compensation of 5^{th} and 7^{th} harmonic components, presents the highest junction temperature. The same behavior is

observed for the diode.

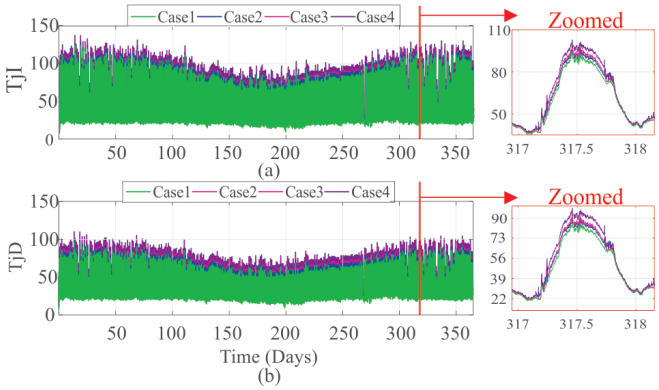

Fig. 14. Mean junction temperature for one year operation considering the long cycles analyzes for (a) IGBT and (b) diode.

The annual lifetime consumption for IGBTs and diodes for the long and short cycles are presented in Table II. As observed, the HCC operation increases the *LC* for the semiconductor devices considering the short and long cycles. In addition, the *LC* values for the short cycle is more significant than these for the long cycles. For the IGBT, compared to the base case (Case 1), it is observed an increasing of 30.76 %, 42.73 % and 48.14 % in the *LC* short cycle for Case 2, Case 3 and Case 4, respectively. With regarding to the diode *LC*, it is observed an increasing of 25.67 %, 43.67 % and 57.81 % in the short cycle *LC* for Case 2, Case 3 and Case 4, respectively. Finally, it is observed that the *LC* values for the diodes are lower than these from the IGBTs.

TABLE II
***LC* considering the short and long cycles.**

Cases	*LC* Short IGBT	*LC* Long IGBT	*LC* Short Diode	*LC* Long Diode
Case 1	0.0351	$2.5422\ 10^{-4}$	$1.2456\ 10^{-2}$	1.4236 10^{-5}
Case 2	0.0459	$5.6542\ 10^{-4}$	$1.5654\ 10^{-2}$	$1.6582\ 10^{-5}$
Case 3	0.0501	$7.3251\ 10^{-4}$	$1.7896\ 10^{-2}$	1.756510^{-5}
Case 4	0.0520	$8.5647\ 10^{-4}$	$1.9658\ 10^{-2}$	1.92310^{-5}

The lifetime evaluation of the dc-link capacitor is also evaluated. The same mission profiles used in the semiconductor devices lifetime analysis were considered. Therefore, the hot-spot temperature over one year is presented in Figure 15.

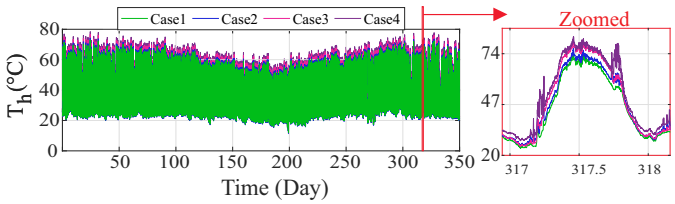

Fig. 15. Hot-spot temperature of one year operation for the dc-link capacitor.

As observed, the HCC increases the hot-spot temperature of the dc-link capacitor compared to the base case (Case 1). The T_h is higher for Case 4, which is the harmonic compensation of the 5^{th} and 7^{th} harmonic components. In this context, the *LC* values for the four cases considering one year mission profile are presented in Table III. As observed, the lifetime consumption increases with the HCC operation. Compared to the base case, there are an increasing of 6.9 %, 8.9 % and 22.23 % for Case 2, Case 3 and Case 4, respectively.

TABLE III
***LC* for the dc-link capacitor considering one year mission profile.**

Cases	*LC*
Case 1	0.0301
Case 2	0.0322
Case 3	0.0328
Case 4	0.0370

Since the lifetime consumption of each element over one year was performed, the Monte Carlo simulation analysis is applied to have a better understanding of the inverter lifetime evaluation. Firstly, the unreliability function $F(x)$ for the system level considering the failure of the inverter caused only by a specific component is performed. The $F(x)$ curve for each component is presented in Figure 16. In addition, the B_{10} values in years for each component are presented in Table IV.

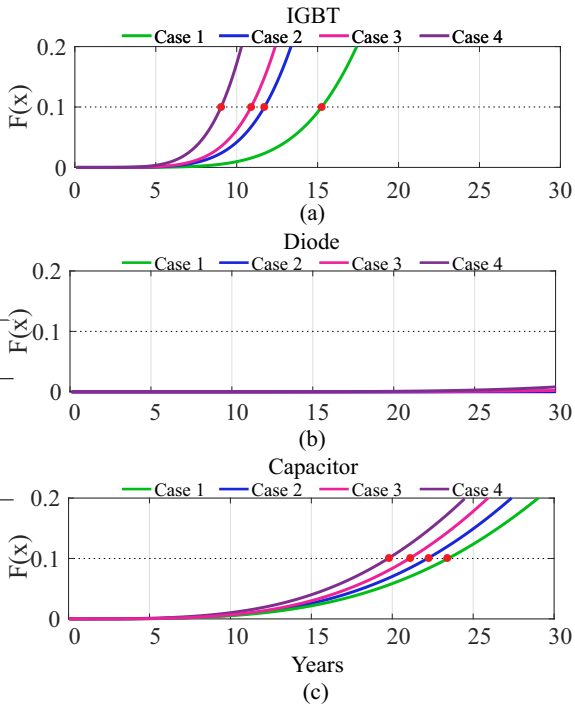

Fig. 16. Unreliability function considering the system level composed of: IGBTs (a), diodes (b) and dc-link capacitors (c).

As shown in Figure 16(a), considering the $F(x)$ for the inverter based on the IGBT, it is observed reduction in the B_{10} due to the HCC operation. Compared to the base case, there are a reduction of 3.7, 4.7 and 6.3 years for Case 2, Case 3 and Case 4, respectively. In addition, the B_{10} for the diodes are smaller compared to that from the IGBT. The $F(x)$ for the dc-link capacitor is presented in Figure 16(c). As observed, the B_{10} reduces due to the HCC process. Compared to the base case, there are a reduction in B_{10} of 2.1, 3.3 and 4.1 for Case 2, Case 3 and Case 4, respectively.

Finally, the unreliability functions for the system level

considering all the components are presented in Figure 17. The B_{10} considering all the components in the Monte Carlos simulation is equal to 14.1, 10.7, 10.0 and 8.5 years for Case 1, Case 2, Case 3 and Case 4, respectively. Thus,it is observed a reduction in the reliability of the inverter due to the HCC operation. Compared to the base case, there are a reduction in 3.4, 4.1, and 5.6 years, respectively.

TABLE IV
B_{10}values for each component.

Cases	B_{10} IGBT	B_{10} Capacitor
Case 1	15.4 years	23.9 years
Case 2	11.7 years	21.8 years
Case 3	10.7 years	20.6years
Case 4	9.1 years	19.8years

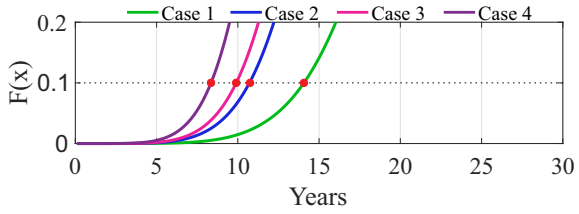

Fig. 17. PV inverter Unreliability function considering the system level.

VII. CONCLUSION

The lifetime evaluation of a 10 kW three-phase PV inverter considering the semiconductors devices (IGBTs and diodes) and dc-link capacitors is performed in this work. The adopted control strategy was implemented in an experimental bench. The lifetime evaluation for short and long cycles analysis considering the mission profiles of solar irradiance, ambient temperature, current harmonic amplitude and phase-angle are performed. The Monte Carlo simulation was used to obtain a more realistic results. The lifetime evaluation of the PV inverter working as traditional operation and the injection of 5^{th} and 7^{th} harmonic components are analyzed.

For the specific case study, the HCC operation reduces the lifetime reliability of the semiconductor devices. The IGBTs and diodes present higher *LC* when the 7^{th} harmonic component is compensated, compared to the 5^{th} harmonic. Also, the *LC* is even higher when the 5^{th} and 7^{th} harmonic components are compensated simultaneously. In addition, lifetime consumption for the diode is lower than that for the IGBT. With regarding to the dc-link capacitor, the same behavior of the semiconductor device was obtained.

Considering the Monte Carlo simulation for the system level, there is a reduction of 3.4 years in the PV inverter (compared to the base case) when only the 5^{th} harmonic component is compensated. Also, there is a reduction of 4.1 years when the PV inverter compensates only the 7^{th} harmonic component. Finally, it is observed a reduction of 5.6 years when the 5^{th} and 7^{th} harmonic are compensated simultaneously.

VIII. ACKNOWLEDGEMENT

This work received financial support from CEMIG-D trough the ANEEL (Brazilian Regulatory Agency) P&D program

REFERENCES

[1] "Renewables 2021: Global Status Report (GRS). 2021.", URL: `http://www.ren21.net8/`.

[2] L. BELLINASO, "Multifunctional Photovoltaic Converters - Classification And Requirements For Grid And Load Compatibility", *Brazilian Journal of Power Electronics*, vol. 21, pp. 139–148, May 2016.

[3] A. M. dos Santos Alonso, L. Carlos Afonso, D. I. Brandao, E. Tedeschi, F. P. Marafão, "Considerations on Communication Infrastructures for Cooperative Operation of Smart Inverters", *in 2019 IEEE 15th Brazilian Power Electronics Conference and 5th IEEE Southern Power Electronics Conference (COBEP/SPEC)*, pp. 1–6, April 2019.

[4] Y. Yang, F. Blaabjerg, H. Wang, M. G. Simoes, "Power control flexibilities for grid-connected multi-functional photovoltaic inverters", *IET Renewable Power Generation*, vol. 10, no. 4, pp. 504–513, April 2016.

[5] H. Nerkar, S. Dhamal, S. Sinha, "Advanced control technique for solar PV plant to provide ancillary services", *in 2016 IEEE Region 10 Humanitarian Technology Conference (R10-HTC)*, pp. 1–6, April 2016.

[6] L. Gusman, H. Pereira, J. Callegari, A. Cupertino, "Design for reliability of multifunctional PV inverters used in industrial power factor regulation", *International Journal of Electrical Power & Energy Systems*, vol. 119, p. 105932, February 2020.

[7] L. Liu, H. Li, Y. Xue, W. Liu, "Reactive Power Compensation and Optimization Strategy for Grid-Interactive Cascaded Photovoltaic Systems", *IEEE Transactions on Power Electronics*, vol. 30, no. 1, pp. 188–202, January 2015.

[8] E. M. da Silveira Brito, A. F. Cupertino, H. A. Pereira, V. F. Mendes, "Reliability-based trade-off analysis of reactive power capability in PV inverters under different sizing ratio", *International Journal of Electrical Power & Energy Systems*, vol. 136, p. 107677, September 2022.

[9] J. Callegari, M. Silva, R. de Barros, E. Brito, A. Cupertino, H. Pereira, "Lifetime evaluation of three-phase multifunctional PV inverters with reactive power compensation", *Electric Power Systems Research*, vol. 175, p. 105873, April 2019.

[10] R. de Barros, E. S. Brito, G. Rodrigues, V. Mendes, A. Cupertino, H. Pereira, "Lifetime evaluation of a multifunctional PV single-phase inverter during harmonic current compensation", *Microelectronics Reliability*, vol. 88-90, pp. 1071–1076, July 2018, 29th European Symposium on Reliability of Elec. Devices, Failure Physics and Analysis (ESREF 2018).

[11] R. C. de Barros, E. M. da Silveira Brito, W. do Couto Boaventura, H. A. Pereira, A. F. Cupertino, "Methodology for bondwire lifetime

evaluation of multifunctional PV inverter during harmonic current compensation", *International Journal of Electrical Power & Energy Systems*, vol. 128, p. 106711, January 2021.

[12] J. Falck, C. Felgemacher, A. Rojko, M. Liserre, P. Zacharias, "Reliability of Power Electronic Systems: An Industry Perspective", *IEEE Industrial Electronics Magazine*, vol. 12, no. 2, pp. 24–35, June 2018.

[13] H. Akagi, E. H. Watanabe, M. Aredes, *Instantaneous power theory and applications to power conditioning*, John Wiley & Sons, May 2017.

[14] H. A. Pereira, G. L. da Mata, L. S. Xavier, A. F. Cupertino, "Flexible harmonic current compensation strategy applied in single and three-phase photovoltaic inverters", *International Journal of Electrical Power & Energy Systems*, vol. 104, pp. 358–369, July 2006, doi: https://doi.org/10.1016/j.ijepes.2018.07.017.

[15] D. Zhou, H. Wang, F. Blaabjerg, "Reactive Power Impacts on LCL Filter Capacitor Lifetime in Grid-Connected Inverter", *IEEE Open Journal of Power Electronics*, vol. 1, pp. 139–148, May 2020.

[16] O. Gandhi, C. D. Rodríguez-Gallegos, N. B. Y. Gorla, M. Bieri, T. Reindl, D. Srinivasan, "Reactive Power Cost From PV Inverters Considering Inverter Lifetime Assessment", *IEEE Transactions on Sustainable Energy*, vol. 10, no. 2, pp. 738–747, June 2019.

[17] A. Anurag, Y. Yang, F. Blaabjerg, "Thermal Performance and Reliability Analysis of Single-Phase PV Inverters With Reactive Power Injection Outside Feed-In Operating Hours", *IEEE Journal of Emerging and Selected Topics in Power Electronics*, vol. 3, no. 4, pp. 870–880, June 2015.

[18] P. D. Reigosa, H. Wang, Y. Yang, F. Blaabjerg, "Prediction of Bond Wire Fatigue of IGBTs in a PV Inverter Under a Long-Term Operation", *IEEE Transactions on Power Electronics*, vol. 31, no. 10, pp. 7171–7182, December 2016.

[19] K. Ma, M. Liserre, F. Blaabjerg, T. Kerekes, "Thermal Loading and Lifetime Estimation for Power Device Considering Mission Profiles in Wind Power Converter", *IEEE Trans Power Electronics*, vol. 30, no. 2, pp. 590–602, Feb 2015.

[20] L. R. GopiReddy, L. M. Tolbert, B. Ozpineci, J. O. P. Pinto, "Rainflow Algorithm-Based Lifetime Estimation of Power Semiconductors in Utility Applications", *IEEE Transactions on Industry Applications*, vol. 51, no. 4, pp. 3368–3375, February 2015.

[21] U. Scheuermann, R. Schmidt, P. Newman, "Power cycling testing with different load pulse durations", *in 7th IET PEMD*, pp. 1–6, April 2014.

[22] H. Huang, P. A. Mawby, "A Lifetime Estimation Technique for Voltage Source Inverters", *IEEE Trans Power Electron*, vol. 28, no. 8, pp. 4113–4119, Aug 2013.

[23] H. Wang, F. Blaabjerg, "Reliability of Capacitors for DC-Link Applications in Power Electronic Converters—An Overview", *IEEE Trans Ind Appl*, vol. 50, no. 5, pp. 3569–3578, February 2014.

[24] J. M. Lenz, J. R. Pinheiro, "Mission Profile Impact on Capacitor Reliability in PV Single-Stage Inverters", *in 7th ICRERA*, pp. 976–981, December 2018.

[25] P. Sundararajan, M. H. M. Sathik, F. Sasongko, C. S. Tan, J. Pou, F. Blaabjerg, A. K. Gupta, "Condition Monitoring of DC-Link Capacitors Using Goertzel Algorithm for Failure Precursor Parameter and Temperature Estimation", *IEEE Trans Power Electron*, vol. 35, no. 6, pp. 6386–6396, Novenmber 2020.

[26] J. Sedo, "Current harmonics compensation in single-phase grid-connected inverter", *in 2018 ELEKTRO*, pp. 1–6, May 2018.

BIOGRAPHIES

Rodrigo Cassio de Barros, received the B.S. degree in electrical engineering from the Universidade Federal de Viçosa (UFV), Viçosa, Brazil, in 2017. He received the M.S. degree in electrical engineering from Federal Center for Technological Education of Minas Gerais, Belo Horizonte, Brazil, in 2019. He is a Substitute Professor with the Department of Electrical Engineering in UFV and a Researcher Assistant with Gerência de Especialistas em Eletrônica de Potência (GESEP). His research interests include power electronics and electrical power systems, with focus in the modular multilevel cascade converters and BESS.

Wallace do Couto Boaventura, Graduated in Electrical Engineering from the Federal University of Minas Gerais (1987), Master's in Electrical Engineering from the Federal University of Minas Gerais (1990) and Ph.D. in Electrical Engineering from the State University of Campinas (2002)., with an internship at the University of Toronto (UofT). He is currently a full professor at the Federal University of Minas Gerais. He has experience in the field of Electrical Engineering, with an emphasis on Electric Power Transmission, Electric Power Distribution, working mainly on the following topics: power systems, electromagnetic compatibility, atmospheric discharge, high voltage and signal processing applications.

Heverton Augusto Pereira, (Member, IEEE) received the B.S. degree from the Federal Federal University of Viçosa (UFV), Viçosa, Brazil, in 2007, the M.Sc. degree from the University of Campinas, Campinas, Brazil, in 2009, and the Ph.D. degree from the Federal University of Minas Gerais, Belo Horizonte, Brazil, in 2015, all in electrical engineering. He was a visiting Researcher from the Department of Energy Technology, Aalborg University, Denmark, in 2014. He has been an Adjunct Professor with the Electric Engineering Department, UFV, since 2009. His main research interests include grid-connected converters for PV and wind power systems, and high-voltage dc/flexible ac transmission systems based on MMC.

Allan Fagner Cupertino, Allan Fagner Cupertino received the B.S. degree in electrical engineering from the Federal University of Viçosa (UFV) in 2013, the M.S. and Ph.D. degrees in Electrical Engineering from the Federal University of Minas Gerais (UFMG) in 2015 and 2019, respectively. He was a guest Ph.D. at the Department of Energy Technology, Aalborg University from 2018 to 2019. Since 2014, he has

been with the Materials Engineering Department at the Federal Center of Technological Education of Minas Gerais (CEFET), where he is currently Assistant Professor. He is a member of the Brazilian Power Electronics Society (SOBRAEP) and Brazilian Society of Automatics (SBA).